

# Monte-Carlo simulations of the broadband X-ray continuum of SS433

Yu. M. Krivosheyev<sup>1,4\*</sup>, G. S. Bisnovaty-Kogan<sup>1,3,4</sup>,  
A. M. Cherepashchuk<sup>2</sup> and K. A. Postnov<sup>2</sup>

<sup>1</sup>*Space Research Institute of Russian Academy of Science (IKI), Profsoyuznaya 84/32, Moscow 117997, Russia*

<sup>2</sup>*Sternberg Astronomical Institute, Moscow State University, Universitetsky pr., 13, Moscow 119992, Russia*

<sup>3</sup>*Joint Institute for Nuclear Research, Joliot-Curie 6, Dubna 141980, Moscow region, Russia*

<sup>4</sup>*Moscow Engineering Physics Institute, Kashirskoe Shosse 31, Moscow 115409, Russia*

2 November 2018

## ABSTRACT

We develop a Monte-Carlo technique based on L.B. Lucy’s indivisible photon packets method to calculate X-ray continuum spectra of comptonized thermal plasma in arbitrary geometry and apply it to describe the broadband X-ray continuum of the galactic superaccreting microquasar SS433 observed by INTEGRAL. A physical model of the X-ray emitting region is proposed that includes thermal emission from the accretion disk, jets and hot corona where the photons of different origin are comptonized. From comparison with INTEGRAL observations, we estimate physical parameters of the complex X-ray emitting region in SS433 and present model spectra for different viewing angles of the object.

**Key words:** X-rays: individual: SS433 – scattering – methods: numerical.

## 1 INTRODUCTION.

SS433 is a peculiar massive X-ray binary system with precessing relativistic jets (Margon 1984). The system is located at a distance of about 5.2 kpc (Lockman et al. 2007) nearly in the galactic plane. The optical companion V1343 Aql was first identified in the survey of stars exhibiting  $H_\alpha$  emission of Stephenson and Sanduleak (1977). It is one of the brightest stars in the Galaxy, the bolometric luminosity of the object assuming isotropic radiation is  $L_{bol} \sim 10^{40}$  erg/s (Cherepashchuk et al. 1982). SS433 is a close binary system with an orbital period of 13.1 days (Cherepashchuk 1981). The uniqueness of this source comes from the presence of narrow oppositely directed subrelativistic jets emitting red and blue-shifted periodically variable lines. The commonly accepted model of SS433 suggests a continuous regime of supercritical accretion of gas onto the relativistic star. The optical star fills its critical Roche lobe supplying powerful and almost continuous flow of gas onto the relativistic star at a rate of  $\sim 10^{-4} M_\odot/yr$  (Fabrika 2004). A supercritical accretion disk forms together with narrow jets of gas propagating perpendicular to the disk plane from the central regions of the disk and having a relativistic speed of 0.26c.

Presently, SS433 is recognized as a galactic microquasar with precessing supercritical accretion disk around a rela-

tivistic compact object, and has been extensively investigated in the optical, radio and X-ray ranges (for a comprehensive review and references see Fabrika (2004)). Masses of both components were obtained from the analysis of the optical light curves of SS433 (Antokhina and Cherepashchuk 1987) and of the hard X-ray eclipses observed by INTEGRAL (Cherepashchuk et al. 2008), so the relativistic object in SS433 is most certainly a black hole. Despite a significant progress in understanding the nature of SS433, the mechanism of collimation and acceleration of matter in jets to the relativistic velocity is still unclear.

In the present paper we shall concentrate on the broadband X-ray spectrum of SS433. In the last years the source was intensively observed by RXTE (Revnivtsev et al. 2004; Filippova et al. 2006), XMM (Brinkmann et al. 2007), Chandra (Marshall et al. 2005) and INTEGRAL (Cherepashchuk et al. 2003, 2004, 2005, 2007). INTEGRAL observations of SS433 discovered a hard X-ray spectrum from the source up to 100 keV visible over the whole precessional period  $\sim 162$  days. This suggests the presence of an extended hot region in the central parts of the supercritical accretion disk (Cherepashchuk et al. 2005, 2007, 2008).

The initial analysis of the broadband X-ray continuum observed by INTEGRAL (Cherepashchuk et al. 2005, 2007) allowed for the first time to estimate the temperature and Thomson optical depth of the assumed hot scattering corona above the accretion disk in SS433. However, the spectral analysis made use of simplifying assumptions about

\* E-mail: krivosheev@iki.rssi.ru (YuMK); gkogan@iki.rssi.ru (GSBK); cher@sai.msi.ru (AMCh); pk@sai.msi.ru (KAP)

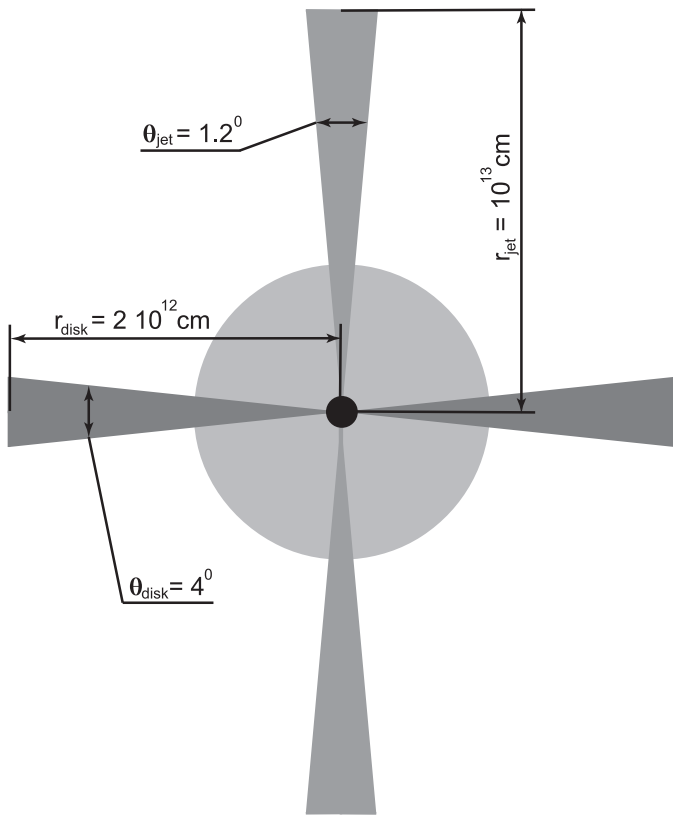


**Figure 1.** Schematic picture of the model adopted for SS433

the corona geometry (mainly because of utilizing the standard models incorporated in the XSPEC tool). The thermal emission from the X-ray jet was treated independently and it was possible to estimate the mass loss rate in the jet. The joint modeling of hard X-ray eclipses and precessional variability allowed the estimation of the size of hot corona in the framework of the adopted geometrical model of the source (Cherepashchuk et al. 2007, 2008). It is well established from observations (see Fabrika (2004) for more detail) and especially from recent studies of X-ray variability of SS433 (Revnivtsev et al. 2004, 2006) that X-ray and optical variabilities are correlated on time scales less than  $10^7$  s. The power spectrum analysis suggests that there is an extended accretion disk with size similar to that in Cyg X-1 in the soft state (Titarchuk et al. 2007). The strong slow wind outflow from the supercritical accretion disk forms a photosphere, and there is a funnel filled with hot plasma around the jet. Clearly, to obtain the correct physical picture, more accurate modeling of the emission processes from the jet, accretion disk and hot corona is needed.

The purpose of this paper is to model the observed broad-band X-ray continuum of SS433 using accurate treatment of emission processes in the jet and the scattering hot corona above the accretion disk. To calculate the broad-band X-ray spectrum, we shall use the Monte-Carlo method (see the Appendix for a more detailed description). The first reason for our choice is connected with the geometry of the system containing the accretion disk, the corona and the jet. This is a rather complicated geometry, it has azimuthal symmetry, but for the outgoing radiation nevertheless it is impossible to obtain any analytical solutions, especially with

account of the temperature decrease along the jet. The second reason is connected with physical processes, in particular the Compton scattering of thermal photons from disk and jet by free electrons in the hot corona. The accurate analytical treatment of this process in the radiation transfer equation makes it impossible to solve it. For the same reasons, the computational algorithm for numerical solution of the transfer equation will be very sophisticated and will demand much computational time. An advantage of the Monte-Carlo method is that the computational algorithm is rather simple. It consists roughly of one procedure repeated many times, and quite a small amount of computational time is required to calculate the emergent spectra with good accuracy. Moreover, when using finite-difference methods, computational errors tend to increase with time as they are accumulated at certain steps of the algorithm. In the Monte-Carlo case the picture is completely different: the precision of the result increases with computational time because of larger number of individual tests and thus better statistics, so waiting longer gives better result.

## 2 GEOMETRICAL MODEL OF SS433

The schematic picture of the source is presented in Fig.1. The collimated, oppositely directed jets were proposed by Fabian and Rees (1979) and Milgrom (1979) to explain the observed moving emission lines at unusual wavelengths. These lines were interpreted as Doppler-shifted Balmer and He I lines (Margon et al. 1979). The morphology of SS433 and the surrounding nebula from radio observations and the analysis of its temporal behavior provides strong support to the idea of ballistically coasting matter ejected from the twin jets, which justifies the so-called "kinematic model" of the jet precession (Abell and Margon 1979) proposed to explain the periodic "movement" of the optical lines. The X-ray imaging observations of Seward et al. (1980) also support the jet model. The jets must be supplied with matter from some source, so a hypothesis of a compact star in a close binary system was proposed. The discovery of the 13-day periodicity in the radial velocity of the "stationary" SS433 emission-line system (Crampton et al. 1980) proved this picture. The donor star fills its critical Roche lobe providing powerful flow onto the compact object. Thus, an accretion disk forms with a pair of narrow jets propagating perpendicular to the disk plane. The presence of the accretion disk follows also from the interpretation of the light curve that involves mutual eclipses of the massive early-type normal star and the extended accretion disk (Cherepashchuk 1981; Antokhina and Cherepashchuk 1987). As was already mentioned in the Introduction, the presence of a hot corona above the inner regions of the accretion disk was suggested to explain the hard X-ray spectrum of SS433 observed by INTEGRAL over the entire precession period (Cherepashchuk et al. 2005, 2007, 2008). So the considered model of SS433 including the accretion disk with hot corona above its central regions and two jets perpendicular to the disk plane is well justified by observations.

## 2.1 Supercritical accretion disk

In SS433, the optical star fills the Roche lobe and supplies matter to the accretion disk at a rate of  $\sim 10^{-4} M_{\odot}/yr$ . The accretion disk radius is assumed to be limited by the size of the Roche lobe and thus for  $M_{bh} = 7M_{\odot}$  and  $q = M_{bh}/M_{opt} = 0.3$  (Antokhina and Cherepashchuk 1987) is  $\sim 10^{12}$  cm. The most emission from the disk is generated in its central regions, so the exact value of the accretion disk radius is of small importance. Far away from the central parts, the standard accretion disk theory (Shakura and Syunyaev 1973) can be used to estimate its geometrical thickness. For the disk height  $h$  growing linearly with radius the disk opening angle  $\theta_{disk}$  can be directly found from the relation:

$$h = r \tan \frac{\theta_{disk}}{2}, \quad (1)$$

We shall consider an optically thick disk, so in our calculations this conical surface will be used as an opaque screen for incident photons. For reasonable input parameters discussed below, the disk opening angle is  $\theta_{disk} = 4^{\circ}$ .

## 2.2 Thermal X-ray jets

The evidence for X-ray emitting jets in SS433 was found in X-ray observations of the source. The *EXOSAT* satellite detected Doppler shifted iron lines moving periodically in accordance with the precessional Doppler curve of the source (Watson et al. 1986), suggesting the X-ray emission origin from the base of jets. Later observations by *Ginga* (Kawai et al. 1989; Brinkmann et al. 1991) and deep *ASCA* observations (Kotani et al. 1994, 1996) discovered many pairs of Doppler-shifted emission lines originating in the blue and red jets moving with a radial velocity of  $0.26c$  (Margon 1984). The soft X-ray emission is fitted by a combination of a thermal bremsstrahlung continuum and emission lines from a multi-temperature optically thin plasma in the conical jets with length  $L_j \sim 10^{13}$  cm and a total X-ray luminosity of  $\sim 3 \times 10^{35}$  erg/s (Kotani 1998). More recent *Chandra* (Marshall et al. 2005; Namiki et al. 2003) and *XMM* observations (Brinkmann et al. 2005) confirmed the basic properties of X-ray jets and put constraints on their geometrical and physical parameters. The much higher kinetic luminosity of jets  $\sim 10^{39} - 10^{40}$  erg/s is derived from their interaction with the surrounding nebula W50 (see Fabrika (2004) for a detailed discussion and further references). We shall assume X-ray jets to have a conical shape, as inferred from the coincidence of the jet opening angle  $\theta_j$  in the optical and X-rays (Fabrika 2004), with the jet opening angle  $\theta_j = 1.2^{\circ}$ .

## 2.3 Hot corona

The presence of a hot corona above the central parts of the accretion disk in SS433 has been suggested by hard X-ray observations of the source by *INTEGRAL* (Cherepashchuk et al. 2005, 2007, 2008). The main indication is the unchanged form of the hard X-ray spectrum at different precession phases. If only thermal emission from cooling jets were responsible for the observed X-rays, one would expect a significant softening of the spectrum at the precessional phase *T3* (disk edge-on), where the innermost hottest parts of X-ray jets are screened by the accretion

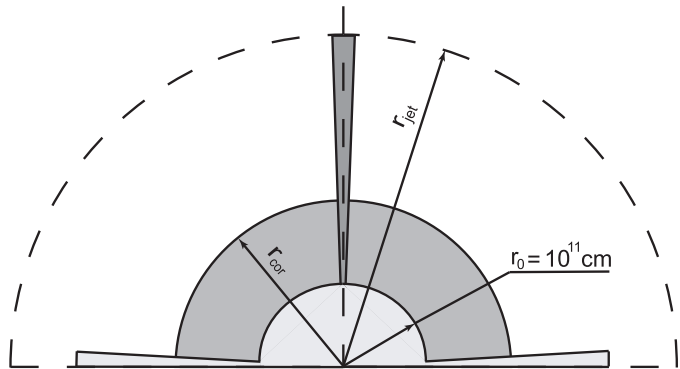


Figure 2. The computational domain.

disk edge. The observed primary X-ray eclipse light curve and precessional hard X-ray variability cannot be successfully described by thermal jets without a broad hot structure above the central parts of the disk which is partially eclipsed at the *T3* precessional phase (Cherepashchuk et al. 2005, 2008). The hard X-ray spectrum at the maximum opening disk phase can be modeled as scattered thermal radiation from jets by an isothermal hot corona ( $T_{cor} \sim 18 - 30$  keV) with spherical or slab geometry using different standard spectral tools from the XSCPEC package (see, for example, Cherepashchuk et al. (2007) for the ComPS model fit). The corona around jets can be heated up to such temperatures, for example, by the interaction of the precessing jets with wind outflow from the supercritical accretion disk (Begelman et al. (2006)). Motivated by additional geometrical constraints obtained from the analysis of the joint precessional and eclipsing X-ray variability of SS433 which suggests a fairly broad opening angle of the jet funnel, we shall assume a spherical shape of the corona. The parameters of the model are shown in Fig.1.

## 3 PHYSICAL MODEL OF THE X-RAY EMITTING REGIONS IN SS433

We consider the accretion disk with a spherical corona above its inner regions, and two jets propagating perpendicular to the disk plane. This picture is symmetric with respect to the disk plane, so we shall consider only its upper half (Fig.1). The system is axially symmetric with respect to the jet axis, so radial profiles of physical quantities fully characterize this 3-dimensional structure. The computational domain (see Fig.2) is bounded by the surface of the accretion disk (from bottom) and a sphere with radius equal to the jet height. The inner accretion disk is assumed to have constant  $h/r$  ratio, so the disk surface is inclined by  $2^{\circ}$  to the equatorial plane. The conical jet, disk and corona begin at the coordinate origin. Both jet and corona are assumed to consist of fully ionized hydrogen plasma. Guided by observations of the accretion wind photosphere (Fabrika 2004; Revnivtsev et al. 2004), we set the visible jet base at  $r_0 = 10^{11}$  cm and assume the inner spherical boundary of the corona to lie at the same radius, as shown in Fig.2.

### 3.1 The jet

We fix the jet opening angle at 1.2 degrees. The temperature at the base of the jet is assumed to be the same as that of the corona and is set to be  $T_0 = 19keV$ , the best-fit value found in our calculations.

$$T = T_0 \left( \frac{r_0}{r} \right)^{4/3}, T \sim \varrho^{2/3}, \varrho \sim r^{-2} \quad (2)$$

In our simulations we shall assume that the jet temperature changes with height according to the law corresponding to the jet cooling due to adiabatic expansion of ideal monoatomic gas (2). In the paper of Koval' and Shakura (1989) an analytic solution for the jet temperature profile was obtained taking into account both adiabatic and approximate treatment of free-free emission cooling. For the constant jet opening angle the solution obtained by Koval' & Shakura is determined by the mass rate in the jet,  $\dot{M}_j$ . If  $\dot{M}_j \geq \dot{M}_{lim} = (5 \cdot 10^{20})^{-1} \cdot 2\pi(1 - \cos \theta_{jet}/2) \mathcal{R} \sqrt{T_0} (0.26c)^2 r_0$ , rapid cooling of the jet plasma occurs. Here  $\mathcal{R}$  is the universal gas constant and  $T_0 = T_{cor}$  is the temperature at the base of the jet. For jet parameters considered by us  $\dot{M}_{lim} \simeq 5.3 \cdot 10^{18}$  g/s. From observations, the kinetic luminosity of the jet is about  $L_{kin} \sim 10^{39-40}$  erg/s (Fabrika (2004)), so the lower limit for the mass loss rate in the jet is  $\dot{M}_j = 3 \cdot 10^{19}$  g/s, which is six times greater than  $\dot{M}_{lim}$ . For  $\dot{M}_j / \dot{M}_{lim} < 1$  the jet cooling occurs almost as in the adiabatic case, but in the opposite case,  $\dot{M} / \dot{M}_{lim} > 1$ , the jet begins to cool rapidly with radius and its total X-ray luminosity should be so small that it would be impossible to observe it. The jet can have a larger opening angle so that the value of  $\dot{M}_{lim}$  increases and may exceed  $\dot{M}_j$ , which will prevent the jet from rapid cooling. There could be also some processes (Compton heating by hard quanta from the corona, interaction with the wind from the disk during the jet precession, etc.) that additionally heat the jet and prevent it from rapid cooling. The accurate treatment of the jet heating has not been done yet, so we assume the adiabatic temperature distribution along the jet.

The density dependence along the jet follows from the continuity equation. The jet mass outflow rate  $\dot{M}_j = nm_p V S$ , where  $n$  is the number density of protons at  $r$ ,  $m_p$  is the proton mass,  $V = 0.26c$  and  $S = \pi r^2 \tan^2 \theta_{jet}/2$  is the jet cross-section. So we can write

$$n = n_0 \left( \frac{r_0}{r} \right)^2, \quad (3)$$

where

$$n_0 = \frac{\dot{M}_{jet}}{\pi m_p V r_0^2} \tan^2 \frac{\theta_{jet}}{2}, \quad (4)$$

### 3.2 The corona

The existence of hot coronas above highly luminous accretion disks was first studied by Bisnovatyι-Kogan and Blinnikov (1976, 1977), where two mechanisms responsible for corona formation have been considered. The first one is connected with disk radiation pressure. The particle moving in the vicinity of a radiating disk suffers the action of radiation from the whole disk. Thus, the radiation force depends on the position of the particle and is maximal at the central

parts of the disk. When the disk luminosity approaches the value of  $\sim 0.6$  Eddington limit, the radiation force exceeds the gravitational one and the outflow from the central parts of the disk sets in. The convection motions in the disk generate acoustic flux, which dissipates in the upper layers of the disk and heats them. As a result, a hot ( $T \sim 10^9$  K) rarefied corona is formed above the central parts of the accretion disk. The second mechanism with account for magnetic field was studied by Galeev et al. (1979). It is connected with magnetic field amplification in the disk. The magnetic field generated by differential rotation of conductive media is amplified due to convective motions in the direction perpendicular to the disk plane. The amplified field can attain strength comparable to equipartition value and magnetic flux will emerge from the disk, leading to formation of accretion disk corona, which consists of many magnetic loops, the fields of which provide an energy source for the corona heating. The corona is hot and has a low density compared to the accretion disk. In the present paper we assume a spherical isothermal corona with temperature  $19keV = 2.2 \cdot 10^8$  K. For simplicity, the radial density dependence in the corona is assumed to obey the same law as in the jet but with the different initial value at  $r = 10^{11}$  cm. Then the optical depth for Thomson scattering in the corona is

$$\tau_{cor} = \sigma_T n_0 \int_{r_0}^{r_{cor}} \frac{r_0^2}{r^2} dr \quad (5)$$

The radius of the corona can be expressed in terms of its optical depth as

$$\begin{aligned} r_{cor} &= r_0 / \left( 1 - \frac{\tau_{cor}}{\sigma_T n_{cor} r_0} \right) \\ n_{cor} &= (4.3 - 4.8) \cdot 10^{12} cm^{-3} \\ \sigma_T &= 6.65 \cdot 10^{-25} cm \end{aligned} \quad (6)$$

The analysis of the observed wide primary orbital hard X-ray eclipse and the precessional variability (Cherepashchuk et al. 2007, 2008) suggests large visible size of the hot corona comparable to that of the accretion disk, but it is not absolutely certain. We have fitted the observed X-ray spectra with two models of corona: 1) the corona is not eclipsed by the precessing accretion disk and has  $r_{cor} = 6.4 \cdot 10^{11}$  cm,  $\tau_{cor} = 0.24$ ; 2) the corona is fully eclipsed with  $r_{cor} = 2.7 \cdot 10^{11}$  cm,  $\tau_{cor} = 0.20$ . Both models can reproduce the observed X-ray spectrum, but the first model gives a slightly better fit. We shall discuss in more detail the obtained results below.

### 3.3 The accretion disk

Basic parameters of the standard accretion disk model include the mass of the compact object  $M$ , mass accretion rate through the disk  $\dot{M}$ , and the angular momentum transport efficiency parameter  $\alpha$ . We are interested in the 'effective' mass accretion rate through the disk and it is different from the mass rate supplying by the optical star through the inner Lagrangian point. The jet kinetic power is approximately equal to the Eddington luminosity for the central black hole mass  $M_{bh} = 7M_\odot$ . This power corresponds to the critical accretion mass rate through the disk  $\dot{M}_{cr}$ .

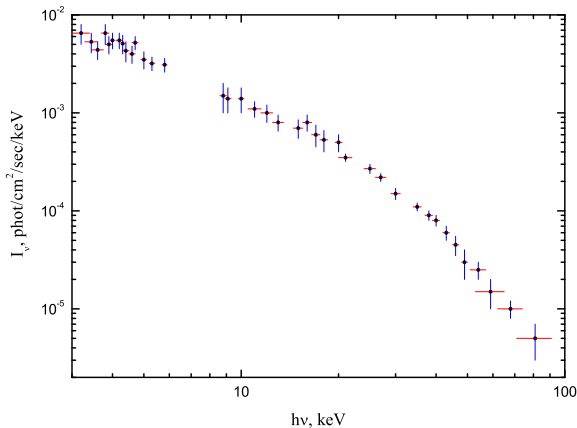


**Figure 3.** X-ray continuum of SS433 from 3 to 90 keV

As the same mass rate should reach the central source to be ultimately consumed by the black hole, the 'effective' mass flow rate through the disk is  $\dot{M} \approx 2\dot{M}_{cr}$ . Taking  $M = 7M_{\odot}$ ,  $\dot{M} \approx 2\dot{M}_{cr}$  and  $\alpha = 0.1$  we obtain that in the outer gas-dominated region with free-free opacity (Shakura and Syunyaev 1973), which lies beyond the radius  $r_{bc} = 4 \cdot 10^{10}$  cm for the adopted parameters,

$$h = 6.1 \cdot 10^3 \alpha^{-1/10} \left( \frac{\dot{M}}{\dot{M}_{cr}} \right)^{3/20} \left( \frac{M}{M_{Sun}} \right)^{9/10} \left( \frac{R}{3R_g} \right)^{9/8} \left[ 1 - \left( \frac{R}{3R_g} \right)^{-1/2} \right]^{3/20} \quad (7)$$

At the accretion disk radius  $R_{disk} = 1.5 \cdot 10^{12}$  cm the half-thickness of the disk is  $5.5 \cdot 10^{10}$  cm, so the angle between the disk surface and the equatorial plane in (1) is  $\theta_{disk}/2 \approx 2^\circ$ . To calculate the emergent photon spectrum from the corona, we shall assume that all accretion disk radiation is emitted only in the central region, from a sphere with radius  $r_0$ , while the outer regions of the accretion disk play the role of an opaque screen for photons (Fig.2). Accretion disk photons are distributed uniformly across the sphere with radius  $r_0$  and initially move strictly in radial direction.

## 4 RESULTS OF SIMULATIONS

### 4.1 Observational data

For spectral analysis, we have made use INTEGRAL observations of SS433 in May 2003 obtained simultaneously by IBIS/ISGRI (20-100 keV) and JEM-X (3-20 keV) telescopes (Cherepashchuk et al. 2003, 2005). The source was observed near the precessional phase 0 (the T3 moment) when the accretion disk is maximally open and the flux from the source is also maximal. The angle between the line of sight and the blue jet (i.e. the jet pointing to the observer) at this phase is  $\approx 60^\circ$ . The Doppler redshift at this precessional phase is  $z \simeq -0.1$ . Spectral lines near 7 keV were ignored. The X-ray data were processed using the standard OSA 5.1

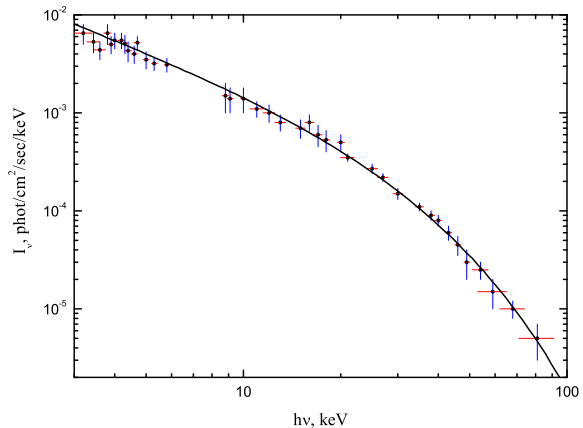


**Figure 4.** The comparison of the Monte-Carlo simulated X-ray continuum of SS433 with observations.  $\theta_{obs} = 60^\circ$ , only the jet and corona emission are considered. The radius of spherically-symmetric corona is  $r_{cor} = 6.4 \cdot 10^{11}$  cm, the mass loss rate in the jet is  $\dot{M}_{jet} = 4 \cdot 10^{19}$  g/s. The viewing angle of the system is  $\theta_{obs} = 60^\circ$ .

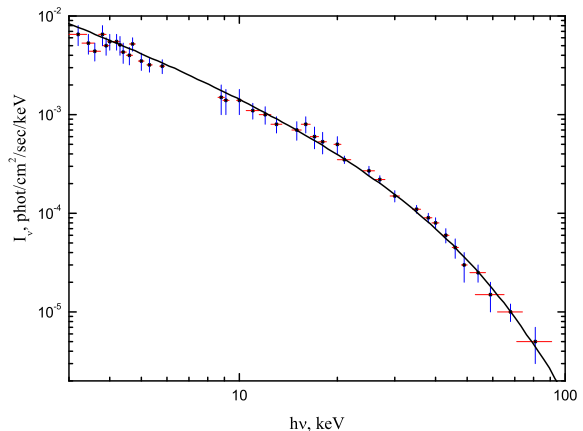


**Figure 5.** The same as in Fig. 4 for smaller corona with  $r_{cor} = 2.7 \cdot 10^{11}$  cm, and  $\dot{M}_{jet} = 3 \cdot 10^{19}$  g/s, viewed by the same angle  $\theta_{obs} = 60^\circ$ .

INTEGRAL software developed by the INTEGRAL science data center (ISDC, <http://isdc.unige.ch> (Courvoisier et al. 2003)). The resulting 3-90 keV X-ray spectrum is shown in Fig.3.

A model fit of the observed spectrum is accepted by achieving the minimal reduced  $\chi^2$  ( $\chi^2_{red} = \chi^2/N$ ),  $N = n - n_{par}$  is the number of the degrees of freedom, see Zombeck (2006).

### 4.2 Bremsstrahlung comptonization model

In this section we present the results of X-ray spectral modeling neglecting the radiation from the disk. The distance to

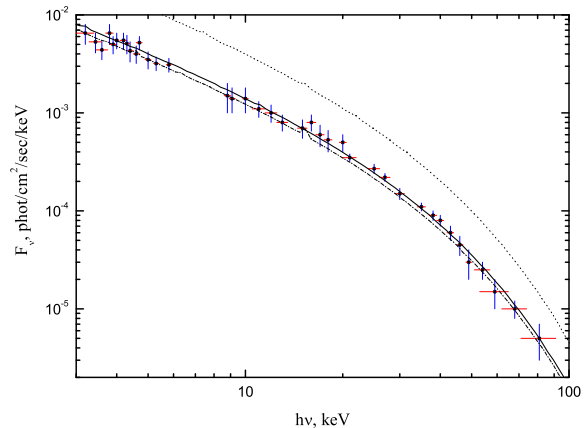
Parameter	Eclipsing corona	Non-eclipsing corona
$r_{cor}, \cdot 10^{11}$ cm	2.7	6.4
$\tau_{cor}$	0.24	0.20
$n_{cor}, \cdot 10^{12} cm^{-3}$	4.8	4.3
$\dot{M}_j, \cdot 10^{19}$ g/s	3	4
$L_{kin}, \cdot 10^{39}$ erg/s	0.9	1.2
$\chi^2$	21.40	23.34
CL	91.6%	95.4%

**Table 1.** Physical parameters of two corona models

SS433 is fixed at  $d = 5$  kpc =  $1.5 \cdot 10^{24}$  cm. The emerging X-ray spectrum in the 3-90 keV range is assumed to be formed due to free-free emission of corona and jet with account for Compton scattering. After many trials, the following best-fit parameters of the model have been obtained (quantitative characteristics of the fitting are discussed in the next paragraph). The temperature of the corona and the jet base is  $T_{cor} = 19$  keV. Fig.4 shows the comparison of the computational results with the observed broadband X-ray spectrum of SS433 for a corona with  $r_{cor} = 6.4 \cdot 10^{11}$  cm,  $\tau_{cor} = 0.24$ ,  $n_{cor} = 4.3 \cdot 10^{12} cm^{-3}$  which is not fully eclipsed by the disk. The mass loss rate in the jet is  $\dot{M}_j = 4 \cdot 10^{19}$  g/s, which corresponds to the kinetic luminosity of  $L_{kin} = 1.2 \cdot 10^{39}$  erg/s. The next Fig.5 shows the results of simulations for a fully eclipsing corona with radius  $r_{cor} = 2.7 \cdot 10^{11}$  cm, the Thomson optical depth  $\tau_{cor} = 0.2$ , and the number density  $n_{cor} = 4.8 \cdot 10^{12} cm^{-3}$ . The mass loss rate in the jet is  $\dot{M}_j = 3 \cdot 10^{19}$  g/s corresponding to the jet kinetic luminosity  $L_{kin} = 9 \cdot 10^{38}$  erg/s.

It is clearly seen that in both cases the model can describe the observed X-ray continuum. The data includes 39 experimental points. There are 5 fitting parameters: the jet mass loss rate  $\dot{M}_j$ , the coronal temperature  $T_{cor}$ , number density at  $r_0$ ,  $n_{cor,0}$ , the Thomson optical depth  $\tau_{cor}$ , and the initial radius  $r_0$ , so the number of the degrees of freedom is  $N_{dof} = 34$ . For the model with non-eclipsing corona  $\chi^2 = 21.4$  shown in Fig. 4 the reduced  $\chi^2_{red} = 0.630$ , and the confidence level of the fit at  $N_{dof} = 34$  is  $\approx 95.4\%$ . For the second model with fully eclipsing corona shown in Fig. 5  $\chi^2 = 23.34$  for 34 degrees of freedom, so the reduced  $\chi^2_{red} = 0.687$  and the corresponding confidence level of the fit is  $\approx 91.6\%$ . Thus the model with non-eclipsing corona (Fig.4) with smaller  $\chi^2$  seems to be more realistic. All model parameters are listed in Table 4.2.

The angular dependence of the emergent X-ray spectrum is shown in Fig.6. The spectrum calculated for the viewing angle  $82^\circ$  is similar to  $60^\circ$ , the minimum viewing angle of the jet during its precessional motion. The weak dependence on the viewing angle may be due to the corona (which radiates almost isotropically) mainly contributing to the total emission at all angles. This figure also shows that the flux from the system is at maximum for the viewing angle  $90^\circ$  when both jets and both parts of the corona contribute to the emergent spectrum. The observations, however, suggest that the flux from the source at this precessional phase (the moment T1, disk edge-on) is minimal. This may indicate that the supercritical accretion disk should be much thicker geometrically than predicted by the standard model Shakura and Syunyaev (1973). Significant screening of the corona by a thick disk is needed to explain the

**Figure 6.** The two-component model spectra of SS433 calculated for different viewing angles: 60 degrees (the bold solid line), 82 degrees (the dash-dotted line), 90 degrees (the dotted line). The emergent spectrum for 90 degrees was obtained by doubling the computational data because of equal contribution of both jets and coronas.  $r_{cor} = 6.4 \cdot 10^{11}$  cm,  $M_{jet} = 4 \cdot 10^{19}$  g/s.

observed precessional variability of SS433 in hard X-rays (Cherepashchuk et al. 2007, 2008).

The calculated spectrum of the source does not vary significantly with the viewing angle in the allowed range  $\theta_{obs} = 60^\circ - 90^\circ$ , but if we were looking straight along the jet ( $\theta_{obs} = 0^\circ$ ), we would observe a completely different picture (Fig.7). Fabrika et al. (2004, 2006) argued that ultraluminous X-ray sources (ULX) are superaccretors like SS433 seen almost along the jet. This hypothesis is based on the following assumptions: the most central parts of the supercritical accretion disk are surrounded by outflowing gas which is semi-opaque, so the 'edge-on' luminosity of such an object should be much smaller than the 'face-on' luminosity, when the hottest central regions are exposed directly. We do not consider the outflowing gas, which is not visible in observational data, so the angular dependence of X-ray luminosity is completely different, as demonstrated above. Moreover, if we were looking straight along the jet, the luminosity would be actually minimal, since along the axis the jet itself is optically thick for its own thermal emission. The thermal energy power emitted per unit volume in the jet decreases with distance as both density and temperature decrease, so the most jet power is released near the jet base. Thus, in order to see the hottest central regions of the accretion disk, the system should be observed not along the jet axis, but slightly from aside, by viewing angles exceeding the jet opening angle.

### 4.3 Influence of the accretion disk emission

The two-component model described in the previous section gives satisfactory results, but the accretion disk emission could also affect the emergent X-ray continuum. To test this in our calculations, we included the emission from the inner parts of the accretion disk with the following spectrum.

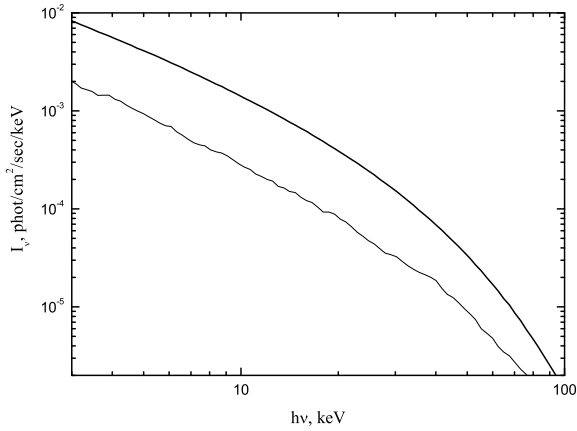


**Figure 7.** The model spectrum of SS433 observed along the jet axis (the solid line) compared with spectrum at  $\theta_{obs} = 60^\circ$  (the bold solid line).

$$\begin{cases} L_\nu = 4L_{disk}/7\nu_c \left(\frac{\nu}{\nu_c}\right)^{1/3}, \nu < \nu_c \\ L_\nu = 4L_{disk}/7\nu_c \exp\left(1 - \frac{\nu}{\nu_c}\right), \nu > \nu_c \end{cases}$$

$$\nu_c = \frac{hT_{ef}}{k}$$

(Here  $L_{disk}$  is the total luminosity of the accretion disk.)

$$T_{ef} \equiv T_{ef}(r_c)$$

The value  $r_c$ , which is interpreted as the inner radius of accretion disk, was taken to be  $r_{sph}/0.3$ , where  $r_{sph} = GMM/L_{cr}$  is the spherization radius (see Shakura and Syunyaev (1973)) at which the disk luminosity equals the critical Eddington luminosity  $L_{cr} = 4\pi cGM_{bh}/\kappa_{es} = 8.8 \cdot 10^{38}$  erg/s. It was shown by Bisnovaty-Kogan and Blinnikov (1977) that the outflow from a supercritical accretion disk begins at  $L_d = 0.6L_{cr}$ . Here we take the lower luminosity of the disk  $L_d = 0.1L_{cr}$ . This may be justified by analysis of complicated physical processes in the supercritical accretion disk, but the main reason for our choice is based on our simulations: at higher  $L_d$  an excess of soft X-rays appears, which is absent in observations. For supercritical accretion the outflow can start from radius where the luminosity is still subcritical, since the disk should be additionally heated by radiation from hot corona. The best fit with the observed spectrum occurs when the luminosity is  $0.1L_{cr}$ . Using the standard disk accretion equations and Paczynski-Witta gravitational potential  $\varphi_{PW} = GM/(r - r_g)$ , the effective temperature can be found to be

$$T_{ef}(r) = 2.05 \cdot 10^7 \left(\frac{\dot{M}}{M_{cr}} \frac{M_{sun}}{M_{bh}}\right)^{1/4} \left(\frac{3r_g}{r}\right)^{3/4} \varphi_{r,r_{in}}^{1/4} \quad (8)$$

Here  $r_{in} = 3r_g$ ,  $r_g = 2GM/c^2$  and  $\varphi_{r,r_{in}}$  is (Bisnovaty-Kogan 1989)

$$\varphi_{r,r_{in}} = \left(1 - \sqrt{\frac{3r_g}{r}}\right)^2 \left(1 - \frac{r_g}{3r}\right) \left(1 + \frac{1}{2}\sqrt{\frac{3r_g}{r}}\right)$$

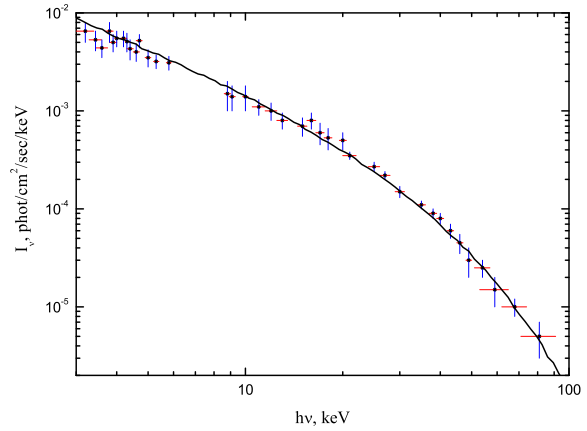


**Figure 8.** The three-component model of SS433 spectrum. The model spectrum is almost identical to the two-component model shown in Fig.5.  $r_{cor} = 2.7 \cdot 10^{11}$  cm,  $M_{jet} = 3 \cdot 10^{19}$  g/s.

$$\left(1 - \frac{r_g}{r}\right)^{-3} \quad (9)$$

For the assumed disk parameters we obtain from these formulas  $T_{ef} \approx 6.0 \cdot 10^5$  K  $\approx 0.05$  keV.

The accretion disk emission is assumed to be emerging from the sphere with radius  $r_0 = 10^{11}$  cm with all photons initially moving radially. Inside this radius  $r_c$  the heat production in the disk exceeds the local Eddington value driving the mass outflow. We assume that  $r_c$  is approximately equal to the inner radius of the jet. We do not take into account the radiation from the region inside  $r_c$ , assuming that it is transformed into the jet energy and heating of the corona. The results of the three-component model simulations are presented in Fig.8 and 9.

It is clear that generally the disk radiation can strongly change the emerging spectrum, but in the energy range 1-100 keV the spectral difference is insignificant because of a comparatively low effective temperature  $T_{ef} \approx 0.05$  keV of the disk emission. In principle, the spectrum at lower energies can be used to estimate the accretion disk physical parameters.

## 5 DISCUSSION

We have developed a Monte-Carlo code for modeling X-ray (3-90 keV) continuum of SS433 based on the realistic physical model of the source, including the accretion disk, thermal jet and hot scattering corona. We found the model parameters that provide good qualitative and quantitative agreement with INTEGRAL observations. The fitting procedure was as follows.

The similarity of hard X-ray spectra of SS433 at different phases of the precessional period, as well as the joint modeling of the orbital primary X-ray eclipse and precessional variability, suggest the presence of a hot corona that is not fully eclipsed by the donor star (Cherepashchuk et al. 2008). This fact allows us to put the lower limit on the outer radius of the corona.

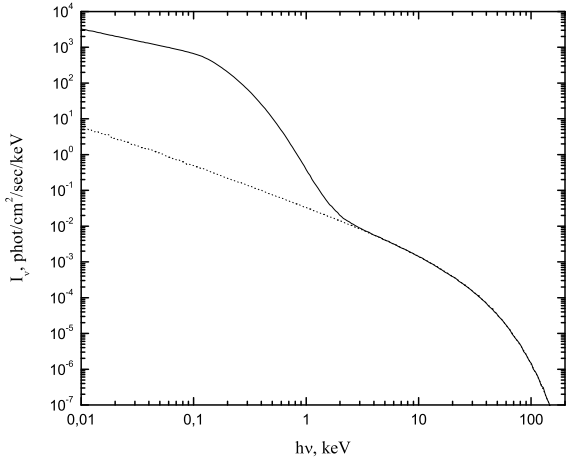


**Figure 9.** Comparison of two- and three-component emission models. The solid curve corresponds to the model with disk radiation, the dashed one – to the model without disk radiation.  $r_{cor} = 6.4 \cdot 10^{11}$  cm,  $\dot{M}_{jet} = 4 \cdot 10^{19}$  g/s.

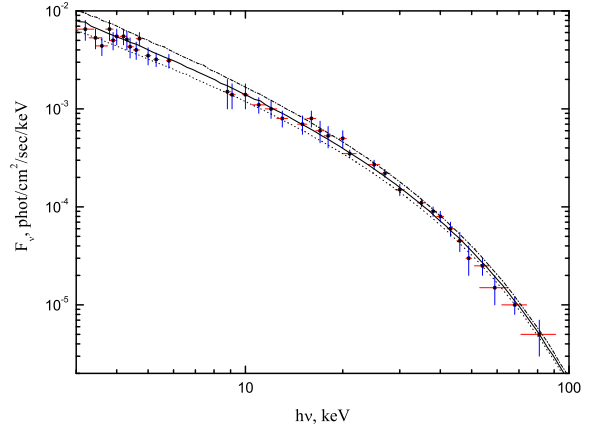


**Figure 11.** The results of the simulations for different values of the jet mass loss rate:  $3 \cdot 10^{19}$  g/s (the dotted line),  $4 \cdot 10^{19}$  g/s (the solid line),  $5 \cdot 10^{19}$  g/s (the dash-dotted line). The best fit is found for  $\dot{M}_{jet} = 4 \cdot 10^{19}$  g/s,  $\tau_{cor} = 0.24$ ,  $T_{cor} = 19$  keV,  $r_{cor} = 6.4 \cdot 10^{11}$  cm.

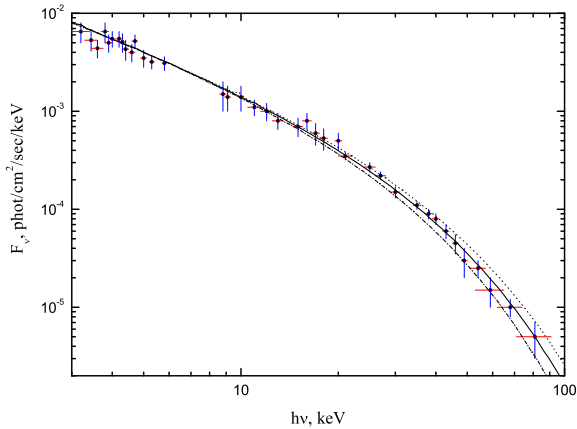


**Figure 10.** The results of the simulations for different coronal temperatures: 17 keV (the dash-dotted line), 19 keV (the solid line), 21 keV (the dotted line). The best fit is found for  $T_{cor} = 19$  keV,  $\tau_{cor} = 0.24$ ,  $r_{cor} = 6.4 \cdot 10^{11}$  cm,  $\dot{M}_{jet} = 4 \cdot 10^{19}$  g/s.

First, we adjust the shape of the spectrum in hard X-rays by varying the coronal temperature, as shown in Fig.10. It is seen from this figure that the coronal temperature affects the hard X-ray spectrum, but does not change the soft X-ray continuum. In opposite, the change of  $\dot{M}_{jet}$  affects the form of only the soft X-ray spectrum (Fig.11) and the hard X-ray is left unchanged, so we can infer the jet mass-loss rate  $\dot{M}_{jet}$  by adjusting the spectrum in the soft X-rays (the temperature of the jet base is assumed to be equal to that of the corona). Note that the change of both jet and corona parameters cannot compensate each other because the related spectral components affect the resulting spectrum in different energy ranges. After that, we adjust the corona op-

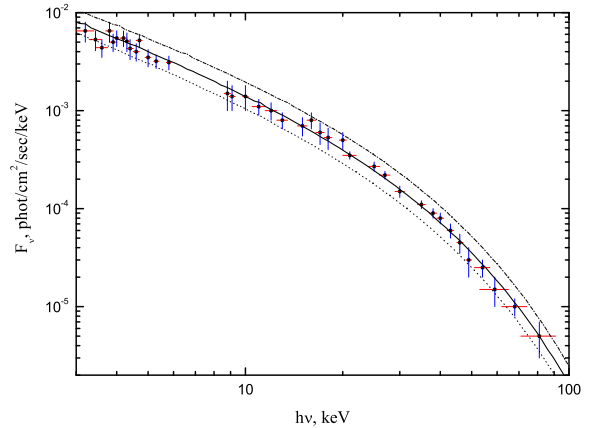


**Figure 12.** The results of the simulations for different optical depth of the corona: 0.2 (the dotted line), 0.24 (the solid line), 0.3 (the dash-dotted line). The best fit is found for  $\tau_{cor} = 0.24$ ,  $T_{cor} = 19$  keV,  $r_{cor} = 6.4 \cdot 10^{11}$  cm,  $\dot{M}_{jet} = 4 \cdot 10^{19}$  g/s.

tical depth (Fig.12). The variations of coronal optical depth at  $\tau_{cor} < 1$  do not change the form of the spectrum, but do change the coronal X-ray luminosity. So we fit the luminosity of the coronal component as shown in Fig.12. Finally, we constraint the accretion disk emission temperature at which the soft part of the model spectrum is still consistent with observations (Fig.13). When the effective temperature of the accretion disk emission is too high, a soft X-ray excess appears, which is not present in observations. In Fig.14 we present the results of our simulations when the X-ray excess from the accretion disk partially compensates the low energetics of the jet. This figure clearly demonstrates that these



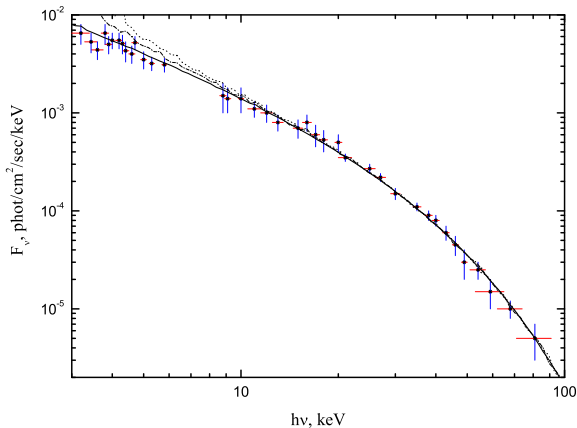


**Figure 13.** The results of the simulations for different values of the accretion disk effective temperature:  $6.0 \cdot 10^5$  K (the solid line),  $9.4 \cdot 10^5$  K (the dash-dotted line),  $1.1 \cdot 10^6$  K (the dotted line). The best fit is found for  $T_{ef} = 6.0 \cdot 10^5$  K,  $\tau_{cor} = 0.24$ ,  $T_{cor} = 19$  keV,  $r_{cor} = 6.4 \cdot 10^{11}$  cm,  $M_{jet} = 4 \cdot 10^{19}$  g/s.

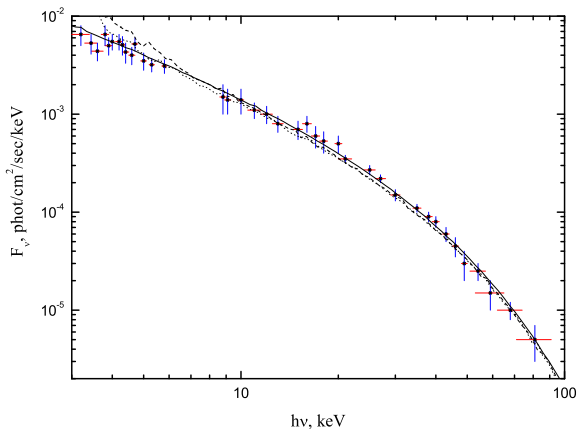


**Figure 14.** Fitting the observational data for a model with low kinetic luminosity of the jet for different values of the accretion disk effective temperature:  $9.4 \cdot 10^5$  K (the dotted line),  $1.1 \cdot 10^6$  K (the dashed line).  $\tau_{cor} = 0.24$ ,  $T_{cor} = 19$  keV,  $r_{cor} = 6.4 \cdot 10^{11}$  cm,  $M_{jet} = 3 \cdot 10^{19}$  g/s. The solid line corresponds to  $T_{ef} = 6.0 \cdot 10^5$  K,  $M_{jet} = 4 \cdot 10^{19}$  g/s with all other parameters as shown for previous lines.

model parameters do not give quantitative agreement with observations.

The last three figures clearly show that the emerging X-ray continuum is very sensitive to slight changes of physical parameters and our results form an island in the parameter space. Further observations and more precise determination of the distance to the source, the component mass ratio, etc., can change the jet mass loss rate and corona density.

We also should stress that the hard X-ray spectrum of SS433 by itself can be formally fitted in several physi-

cal models, ranging from purely thermal emission from jets with changing temperature to variants of standard compotonization procedures from the XSPEC package. An example of such a description with CompPS model is given in Cherepashchuk et al. (2007). However, when the physical parameters of the system are fixed by other observations, like those discussed in this paper, the description of hard X-ray spectrum by standard tools become not self-consistent. So the results of spectral modeling presented in this paper can be considered as a first attempt to find disk, jet and corona parameters in a self-consistent way. Clearly, further observations of the complicated variable emission from SS433 are needed to improve the model parameters.

We would like to draw attention to some recent results in determining the binary component masses in SS433. The optical spectroscopy of the system (Hillwig and Gies 2008; Hillwig et al. 2004) revealed the presence of absorption lines in the spectrum of the optical component identified as a  $\sim$  A7I supergiant star. Observed orbital Doppler shifts of the absorption lines of the optical component allowed Hillwig & Gies to determine the mass ratio of the relativistic ( $M_x$ ) and the optical ( $M_v$ ) components in SS433  $q = M_x/M_v \simeq 0.3 \pm 0.11$ , implying the masses  $M_x = 4.3 \pm 0.8M_\odot$  and  $M_v = 12.3 \pm 3.3M_\odot$ . These results are not the final ones (cf. the analysis by Cherepashchuk et al. (2008), who obtained  $M_x \sim 5M_\odot$ ), and the values of the binary component masses can change with different interpretation of optical spectroscopic observations, as those authors mention in the conclusion Hillwig and Gies (2008). Nevertheless, the smaller mass of the compact object compared to our choice ( $M_{BH} = 7M_\odot$ ) will result in decreasing of the corresponding Roche lobe size, and thus the accretion disk radius. But X-ray spectral properties of SS433 are determined by jets and corona above central parts of the accretion disk, so the X-ray spectrum of the source will hardly change significantly for smaller  $M_x$ .

We conclude that the observed broadband X-ray continuum of SS433 is dominated by thermal emission of the jet and rarefied hot corona around the inner parts of the supercritical accretion disk, with addition from the inverse Compton scattering on hot electrons of the corona. The jet mostly contributes in the soft X-ray band, while hard X-ray emission is dominated by thermal emission from the corona and inverse Compton scattering of soft thermal X-ray photons. The emission from inner regions of the accretion disk also contributes to the spectrum, but mostly at energies below 1 keV. The observed broadband X-ray spectrum of SS433 is best fitted by the corona temperature  $\simeq 19$  keV with Thomson optical depth  $\tau_{cor} \simeq 0.24$  and the jet mass loss rate about  $4 \cdot 10^{19}$  g/s which corresponds to the kinetic luminosity of the source  $1.2 \cdot 10^{39}$  erg/s.

## 6 ACKNOWLEDGEMENTS

The work is partially supported by the Russian Foundation for Basic Research under grants 08-02-08494, 08-02-00491, 06-02-90864, 06-02-91157, by the Russian Federation President's grant for supporting of leading scientific schools NSh-2977.2008.2 and by the RAS Presidium program.

The authors would like to thank A.G. Doroshkevich and

B.E. Stern for useful discussion and the anonymous referee whose remarks helped us to improve the paper.

## 7 APPENDIX: MONTE-CARLO TECHNIQUES

The Monte-Carlo method has another name: the statistical test method. An innumerable number of processes can be listed the outcome of which is not determined and has a probabilistic nature. When repeated, they will give us different results. But these processes obey statistical laws that can be ascertained by repeating one process many times, i.e. by performing statistical tests. As the number of tests increases, the fluctuations decrease, and we can evaluate some value that we are interested in. For instance, the mean value of a random variable, its variance, the density probability, etc. The process of photon propagation through a medium has probabilistic character: the photon interacts with matter, this interaction changes the photon properties (e.g. its frequency, the direction of motion) and one cannot predict exactly the outcome of the process, i.e. whether the photon escapes from the medium, where the photon will escape, and its new frequency. Because of that the Monte-Carlo method is suitable for deriving the characteristics of the radiation field, such as its spatial and frequency distribution. Of course, one can solve the radiation transfer equation to obtain these quantities using some approximations for stationary and time-dependent problems, e.g. see Sunyaev and Titarchuk (1980), Titarchuk (1988), but in all cases the geometry of the problem is rather simple and in many cases cannot be applied directly to sources with complex geometry of emitting/scattering regions, like SS433. Also, the finite-difference numerical solution of an integro-differential equation with frequency dependence is quite sophisticated and requires much computational time. These are our reasons for choosing the Monte-Carlo method.

One possible way to perform a single test with a photon is to simulate its trajectory in a medium. Initially a photon is placed somewhere within the computational domain, its frequency and the direction of motion are known, and we trace the photon as it propagates through the medium (below we shall discuss how one can do this). The moment when the photon leaves the computational domain, or its trajectory is terminated, is considered to be the end of the test and the longest time of one test is taken to be the duration of the Monte-Carlo experiment itself  $\Delta t$ . But there is a problem: any real source emits enormous amount of photons, so it will take correspondingly enormous amount of time to simulate all trajectories, and one will have to wait for years to get the result. It is clear that we should abandon real photons and introduce model ones. One possible way is to trace many photons combined in a group, i.e. a photon packet. At this point, another problem arises: when a pack of photons interacts with the medium, some photons are, for example, scattered, others are absorbed or produce an electron-positron pair in the field of an atomic nucleus, or something else. One can split the photon packet and follow the trajectory of each part, but there is another way out. In our simulations we used the indivisible photon packets method developed by Lucy (1999). According to this method, individual photons are grouped in the packets with constant energy

$$\varepsilon_0 = nh\nu. \quad (10)$$

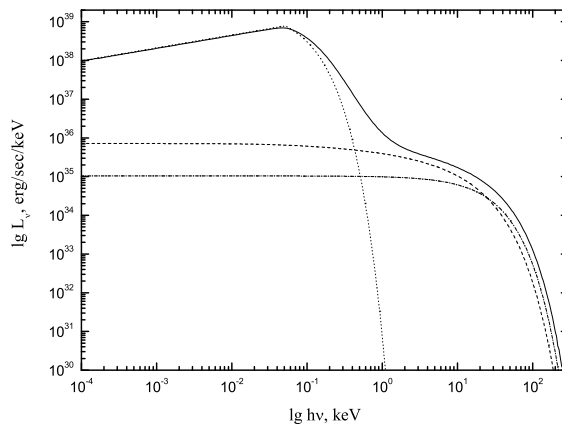


**Figure 15.** Initial spectra: accretion disk emission (dotted line), jet free-free emission (dashed line), corona free-free emission (dash-dotted line). The solid line is the result of the Monte-Carlo simulation. Comptonization of emission on corona electrons is responsible for 'hardening' of the spectrum.

Such a trick helps us to avoid individual tracing of a large number of photons, especially in the low-energy part of the spectrum, since the number of photons in a packet increases with decreasing frequency. The process of interaction of a photon from the packet is chosen each time, according to the known probability of the variant. Such a method may look inexact, but the increasing of the number of photon packets makes less probable things happen, which approaches the result to the exact solution.

### 7.1 The number of photon packets

At the beginning of the Monte-Carlo experiment a number of the photon packets is placed within the computational domain. This number is arbitrary, but the higher this number, the better accuracy can be achieved in the resulting spectrum. As a consequence of the statistical character of the experiment, the relative error in the result is inversely proportional to the square root of the photon packets number, so to increase the accuracy by an order of magnitude one should increase the number of photon packets by two orders of magnitude. About  $10^8$  photon packets is enough to provide a smooth spectral curve that can be compared with observations. In our case there are photon packets of different origin: free-free photons from the jet and corona and the accretion disk photons. Each 'photon type' has its own area of the initial spatial location and spectral distribution. In Fig.15 the initial spectra are presented together with the result of the Monte-Carlo simulation which is discussed in the main text. Each component makes its contribution to the source luminosity. The free-free emissivity of plasma in the jet or corona is

$$L_{ff} = \int dV n_e^2(r) \int d\Omega \int_0^\infty d\nu k_\nu(T) B_\nu(T) \quad (11)$$

It should be taken into account that the temperature varies along the jet, so one should first integrate over the frequency and then over the jet volume. The corona is isothermal and  $L_{ff,cor}$  can be calculated as a product of three integrals. The photon luminosity of the accretion disk was taken to be a fraction of the Eddington luminosity  $L_{disk} = \eta L_{Edd}$  with the factor  $\eta$  being inferred during the fitting procedure.

One should set the number of photon packets  $N$  that will participate in the Monte-Carlo experiment. After calculating the total luminosity of all components

$$L_{tot} = L_{disk} + L_{ff,jet} + L_{ff,cor}, \quad (12)$$

we determine the value  $\varepsilon_0/\Delta t$  as

$$\frac{\varepsilon_0}{\Delta t} = \frac{L_{tot}}{N}, \quad (13)$$

where  $\varepsilon_0$  is the energy of the packet,  $\Delta t$  is the duration of the Monte-Carlo experiment. Once this value is calculated we can determine the number of photon packets representing different spectral components as

$$N_i = \frac{L_i}{\varepsilon_0/\Delta t} = \frac{L_i}{L_{tot}} N. \quad (14)$$

The index 'i' stands for the 'type of emission' (corona or jet free-free or accretion disk emission).

## 7.2 The distribution of photon packets over the frequency bins

The frequency to the photon packet should be assigned. The necessary spectral range is divided into several frequency bins. Their number must be sufficiently high to provide a smooth spectrum, but small enough so that the average number of photons (packets) per bin  $N_{ph}$  be larger than unity,  $N_{ph}/N_{bin} \gg 1$ . In our calculations we divided the spectrum into 500 equal bins on logarithmic scale. The initial frequency was taken in the middle of the frequency bin. The number of photon packets in each frequency bin  $N_{ij}$  is determined by the photon spectral distribution and is proportional to the contribution of the frequency bin to the emissivity of the spectral component:

$$N_{ij}/N_i = \int_{\nu_{j-1}}^{\nu_j} L_{i,\nu} d\nu / \int_0^{\infty} L_{i,\nu} d\nu \quad (15)$$

All photon packets in each frequency bin are assigned the same frequency. During a Monte-Carlo experiment, the trial photons are chosen sequentially starting from the low-frequency bins to the high-frequency ones.

## 7.3 Initial data for photon packets

### 7.3.1 The spatial position

Let us determine the spatial positions of the photon packets. Obviously, in a homogeneous and isothermal medium the free-free photons should be distributed uniformly. But if the medium is inhomogeneous or/and non-isothermal, the situation is more complicated. One should divide the whole volume into regions of constant density and temperature. In the particular case of spherically symmetrical density and

temperature distributions in the corona, the volume was divided into spherical layers with constant density and temperature. The corona was divided into 300 layers of constant thickness, and jet was divided by similar spherical cuts into about  $10^4$  truncated cone layers. The contribution of each layer to the total emissivity was calculated according to (11) and a certain number of photon packets representing the free-free spectrum of each layer was introduced. In each layer its own free-free spectrum was maintained constant. The photon packets within a layer were distributed with equal probability for a free-free photon to appear in each point in the layer

$$\begin{cases} r &= [(r_i^3 - r_{i-1}^3) \gamma_1 + r_{i-1}^3]^{\frac{1}{3}} \\ \cos \theta_{in} &= (\cos \theta_{jet}/2 - \sin \theta_{disk}/2) \gamma_2 + \sin \theta_{disk}/2 \\ \varphi_{in} &= 2\pi \gamma_3 \end{cases}$$

Here  $r_i$  and  $r_{i-1}$  are outer radii of the  $i$ -th layer,  $\gamma_{1,2,3}$  are random numbers distributed uniformly over the interval  $(0, 1)$ ,  $\theta_{jet}$  is the jet opening angle and  $\theta_{disk}$  is the accretion disk thickness angle.

In the case of the accretion disk photon packets, the situation does not differ drastically. They are emitted from the spherical segment with radius  $r_0$ , and should be uniformly distributed over this surface:

$$\begin{cases} r &= r_0 \\ \cos \theta_{in} &= (1 - \sin \theta_{disk}/2) \gamma_2 + \sin \theta_{disk}/2 \\ \varphi_{in} &= 2\pi \gamma_3 \end{cases}$$

### 7.3.2 The initial direction of motion

One should set the initial direction of motion for the photon packets. Free-free photon packets emitted in a plasma move isotropically (Sobol' 1973).

$$\begin{cases} \cos \theta &= 2\gamma_4 - 1 \\ \varphi &= 2\pi \gamma_5 \end{cases}$$

In the Cartesian coordinates, unit vectors (orts) determining the initial direction of motion are written as

$$\begin{cases} e_x &= \sin \theta \cos \varphi \\ e_y &= \sin \theta \sin \varphi \\ e_z &= \cos \theta \end{cases}$$

Initial photon packets from the accretion disk are assumed to move radially.

## 7.4 Simulation of the photon packet trajectory

Simulation of propagation of photons through the medium is the essence of the Monte-Carlo experiment because at this stage the resulting angle and spectral distribution of the photon packets is formed. Once the initial conditions for a photon packet are set, one can find a randomly distributed optical depth the packet must travel before it interacts with matter using a simple Monte-Carlo formula

$$\tau = -\ln \gamma, \quad \gamma \text{ is a random number.} \quad (16)$$

Next, we should choose the velocity and the direction of motion of an electron that scatters the photon packet. For electrons with relativistic Maxwellian distribution, the velocity of electron can be calculated using the random number algorithm suggested by Pozdnyakov et al. (1983).

In the corona all directions of motion are equally probable, so the distribution of orts of the electron motion is isotropic (7.3.2). The matter in the jet moves with the radial velocity  $0.26c$ . The distribution of directions of motion of electrons is isotropic in the local co-moving jet frame. So the resulting vector of motion of an electron is obtained by the Lorentz transformation of the isotropic ort (in the co-moving frame) to the rest frame.

After that the coordinates of the photon-electron interaction point can be found. We determine the total optical depth as

$$\tau = \int dl n_e(r) [\sigma_C + k_\nu(T) n_e(r)] \quad (17)$$

For a given density distribution we can integrate this expression analytically, taking into account that the photon packet trajectory is a straight line defined by the equation

$$\vec{r}_{i+1} = \vec{r}_i + s \vec{e}_v \quad (18)$$

Thus we obtain a transcendental equation for the distance  $s$  the photon travels between two subsequent interactions. This equation is solved numerically using the Newton method. After that we obtain the required coordinates of the interaction point from (18). We must check whether the interaction point lies within the region occupied by plasma (the computational domain). If it does not, then we trace the photon trajectory to the boundary of the computational domain, and collect all necessary information, such as photon's frequency and escape angle.

If the interaction point lies within the computational domain, we should choose the process of interaction of radiation with matter. We assume that the continuum X-ray spectrum of SS433 in the 3-90 keV range is formed due to the Compton scattering by free electrons and free-free absorption/emission, so the choice should be done randomly between these two events. We select the physical event by means of a simple Monte-Carlo procedure. A random number uniformly distributed over the interval  $(0, 1)$  is selected, and if it satisfies the criterion (Lucy 1999)

$$\gamma < \frac{\sigma_C}{\sigma_C + k_\nu(T) n_e(r)} \quad (19)$$

then the photon packet was considered to suffer a Compton scattering, otherwise it was considered to suffer a free-free absorption. If scattering occurs, we should determine the new frequency of the packet and its new direction of motion as in Pozdnyakov et al. (1977). The energy of the photon packet should be changed with the change of frequency according to (10), so the number of photons in the packet remains constant. If the photon packet is absorbed, then it simply disappears, and we proceed to the next packet.

This sequence should be repeated until the photon packet is absorbed or has left the computational domain. Then we gather all required information about the escaped photon packet. To complete the Monte-Carlo experiment, this procedure is applied to all photon packets.

## REFERENCES

- Abell G.O., Margon B., 1979, *Nature*, 279, 701  
 Antokhina E.A., Cherepashchuk A.M., 1987, *Sov. Astron.*, 31, 3, 295  
 Begelman M.C., King A.R., Pringle J.E., 2006, *MNRAS*, 370, 399  
 Bisnovaty-Kogan G.S., 1989, *Physical problems in the theory of stellar evolution*. Nauka, Moscow (in Russian). (English translation: *Stellar Physics*, Vol. 1,2. Springer, 2001)  
 Bisnovaty-Kogan G.S., S.I. Blinnikov, 1976, *SvAL*, 2, 489  
 Bisnovaty-Kogan G.S., Blinnikov S.I., 1977, *AA*, 59, 111  
 Brinkmann W., Kawai N., Matsuoka M., Fink H.H., 1991, *AA*, 241, 112  
 Brinkmann W., Kotani T., Kawai N., 2005, *AA*, 431, 575  
 Brinkmann W., Pratt G. W., Rohr S., Kawai N., Burwitz V., 2007, *AA*, 463, 611  
 Cherepashchuk A.M., 1981, *MNRAS*, 194, 761  
 Cherepashchuk A.M., Aslanov A.A., Kornilov V.G., 1982, *Sov. Astron.*, 26, 697  
 Cherepashchuk A. M., Sunyaev R. A., Seifina, E. V. et al., 2003, *AA*, 411, L441  
 Cherepashchuk A.M., Sunyaev R.A., Fabrika S.N., Molkov S.V. et al., 2004, *Proceedings of the 5th INTEGRAL Workshop*, Munich, 16-20 February 2004, ESA SP-552  
 Cherepashchuk A.M., Sunyaev R.A., Fabrika S.N., Postnov K.A. et al., 2005, *AA*, 437, 561  
 Cherepashchuk A.M., Sunyaev R.A., Seifina E.V. et al., 2007, in *Proc. 6th INTEGRAL Workshop*, Ed. S. Grebenev, R. Sunyaev, C. Winkler, ESA SP-622, p. 319  
 Cherepashchuk A.M. et al., 2008, in preparation; arXiv:0811.0069  
 Courvoisier T.J.-L., Beckmann V., Bourban G., et al., 2003, *AA*, 411, L53  
 Crampton D., Cowley A.P., Hutchings J.B., 1980, *ApJ Lett.*, 235, L131  
 Fabian A.C., Rees M.J., 1979, *MNRAS*, 187, 13  
 Fabrika S., 2004, *Astrophys. Space Phys. Rev.*, 12, 1  
 Fabrika S., Karpov S., Abolmasov P., Shoukulova O. 2004, *Proceedings of IAU Symposium 230*, 1  
 Fabrika S., Abolmasov P., Karpov S. 2006, *Proceedings of IAU Symposium 238*, 1  
 Filippova E., Revnivtsev M., Fabrika S., Postnov K., Seifina E., 2006, *AA*, 460, 125  
 Galeev A.A., Rosner R., Vaiana G.S., 1979, *ApJ*, 229, 318  
 Hillwig T.C., Gies D.R. et al., 2004, *ApJ*, 615, 422  
 Hillwig T.C., Gies D.R., 2008, *ApJ*, 676, 1, L37  
 Kawai N., Matsuoka M., Pan H.C, Stewart G.C., 1989, *PASJ*, 41, 491  
 Koval'E.V. and Shakura N.I., 1989, *Proc. 23rd ESLAB Symp. on Two-Topics in X-Ray Astronomy*, Bologna, Italy, 13-20 September, 1989 (ESA SP-296, Nov. 1989)  
 Kotani T., Kawai N., Aoki T. et al., 1994, *PASJ*, 46, 4, L147  
 Kotani T., Kawai N., Matsuoka M., Brinkmann W., 1996, *PASJ*, 48, 619  
 Kotani T., 1998, *PhD Thesis*  
 Lockman F.J., Blundell K.M., Goss W.M., 2007, *MNRAS*, 381, 881  
 Lucy L.B., 1999, *Astron.Astrophys.*, 344, 282  
 Margon B., 1984, *ARAA*, 22, 507  
 Margon B., Ford H.C., Grandi S.A., Stone R.P.S., 1979, *ApJ Lett.*, 233, L63  
 Marshall H.L., Canizares C.R., Schulz N.S. et al., 2005, *BAAS*, 38, 362  
 Milgrom M., 1979, *AA*, 78, L9  
 Namiki M., Kawai N., Kotani T., Makishima K., 2003,

- PASJ, 55, 281
- Pozdnyakov L.A., Sobol' I.M., Syunyaev R.A., 1977, *Astron. Zh.*, 54, 1246
- Pozdnyakov L.A., Sobol' I.M., Syunyaev R.A., 1983, *Soviet Scientific Reviews, Section E: Astrophysics and Space Physics Reviews*, 2, 189. Translation.
- Revnitsev M., Burenin R., Fabrika S. et al., 2004, *AA*, 424, L5
- Revnitsev M., Fabrika S., Abolmasov P., Postnov K. et al., 2006, *AA*, 447, 545
- Seward F., Grindlay J., Seaquist E., Gilmore W., 1980, *Nature*, 287, 806
- Shakura N.I., Syunyaev R.A., 1973, *Astron.Astrophys.*, 24, 1973
- Sobol'I.M., 1973, *Numerical Monte-Carlo Methods*. Nauka, Moscow (in Russian).
- Stephenson C.B., Sanduleak N., 1977, *ApJ Suppl. Ser.*, 33, 459
- Sunyaev R.A., Titarchuk L.G., 1980, *AA*, 86, 121
- Titarchuk L.G., 1988, *Ap*, 29, 2, 634
- Titarchuk L., N. Shaposhnikov, V. Arefiev, 2007, *ApJ*, 660, 556
- Watson M.G., Stewart G.C., Brinkmann W., King A.R., 1986, *MNRAS*, 222, 261
- Zombeck M.V., *Handbook of Astronomy and Astrophysics*, 3rd edition, Cambridge University Press, 2006

This paper has been typeset from a  $\text{\TeX}$ / $\text{\LaTeX}$  file prepared by the author.